Modeling of Temperature Swing Effect in Silica Reinforced Porous Anodized Aluminum Based Thermal Barrier Coating

Abhilash Gulhane[1], Jian Zhang[1], Xuehui Yang[1], Zhe Lu[2], Hye-Yeong Park[3], Yeon-Gil Jung[3], Yafeng Li[1], Jing Zhang[1]

1. Department of Mechanical and Energy Engineering, Indiana University – Purdue University Indianapolis, Indiana, USA
2. School of Materials and Metallurgical Engineering, University of Science and Technology of Liaoning, China
3. Department of Materials Convergence and System Engineering, Changwon National University, Changwon, Republic of Korea

Abstract

This paper presents a finite element (FE) based model to simulate the temperature swing phenomenon of Silica Reinforced Porous Anodized Aluminum (SiRPA) thermal barrier coatings (TBCs). A realistic 3D SiRPA coating microstructure is constructed, based on the morphology of an experimentally grown coating structure, and the known relationship of geometry and anodization parameters. The coatings' thermophysical properties are first computed using the FE model. The predicted thermal conductivity, thermal diffusivity, and bulk density are compared well with the experimental values. Also, transient thermal analysis is conducted to model the temperature swing effect of the coating by comparing the temperature fluctuation of SiRPA coating with conventional Yttria Stabilized Zirconia (YSZ) based TBCs. With the predicted thermophysical properties, the model is capable to predict the "temperature swing" effect of SiRPA by a transient thermal analysis. Temperature fluctuation of SiRPA is found greater compared to YSZ coating, suggesting its applicability in internal combustion engines. The porosity-dependent thermal conductivity of SiRPA coating is numerically derived. The thermal conductivity decreases linearly with increasing total porosity. The modeling data illustrate that the

This is the author's manuscript of the article published in final edited form as:

Gulhane, A., Zhang, J., Yang, X., Lu, Z., Park, H., Jung, Y., Li, Y., & Zhang, J. (2021). Modeling of Temperature Swing Effect in Silica-Reinforced Porous Anodized Aluminum-Based Thermal Barrier Coating. SAE International Journal of Materials & Manufacturing, 14(3), 283–292.

SiRPA coating shows a higher fluctuation compared to YSZ based TBCs, suggesting its applicability in internal combustion engines.

Keywords: Modeling; Silica Reinforced Porous Anodized Aluminum; SiRPA; Thermal barrier coating

1. Introduction

A continuous effort to increase engine efficiency and stringent emission norms to reduce carbon dioxide and particulate matter emissions globally has led to higher demand to improve engine efficiency. In an internal combustion engine (ICE), a various loss that impacts the efficiency is due to friction, pumping system, exhaust, and heat.

Reducing heat losses can play an important role in increasing efficiencies [1]. Heat transfer through the boundaries shows a significant effect in determining the overall performance of ICEs [1]. The heat losses through the boundaries reduce the overall pressure and temperature of gases resulting in lower work output [1]. It is suggested that almost 50% of the total heat loss occurs through the piston. Heat losses are strong functions of thermal gradients that vary spatially and temporally [1, 2].

Inagaki *et al.* proposed a new concept of diesel combustion that uses a highly dispersed spray with restricted in-cylinder swirl and squish flows. This approach reduces the heat transfer coefficient to achieve low emissions and high efficiencies by minimizing cooling losses [3, 4]. Matsuoka *et al.* used a low thermal conductivity (k) ceramic material to construct a heat-insulated engine with no cooling system and demonstrated its reliability. However, this method had adverse effects on the exhaust gas characteristics because intake heating and higher in-cylinder temperature promoted NOx formation. It also reduced the ignition delay for the diesel spray, causing increased soot formation [5, 6].

An alternative approach that may alleviate these problems has recently been proposed, which is based on coating the combustion chamber walls with a material having a low specific heat capacity and thermal conductivity known as Thermal Barrier coating (TBCs)[6]. For TBC approaches, while increased wall surface temperatures can help to reduce heat losses, however, they tend to have unfavorable effects on the onset of knock-in spark-ignited engines[6]. As a result, the piston surfaces have shown invariably high surface temperatures both during the intake and compression strokes, leading to preheating air during the intake stroke leading to an increase in the working gas temperature and thereby decreasing the volumetric efficiency. This leads to a decrease in the charging efficiency, as well as knocking in gasoline engines [7].

To address this issue in conventional TBCs, Silica Reinforced Porous Anodized Alumina (SiRPA) coatings were developed, which respond rapidly to the fluctuating in-cylinder gas temperatures [8]. This rapid fluctuation phenomenon is named as ‘Temperature Swing’ effect, as illustrated in Figure 1. As a result, the SiRPA coated surface reaches higher peak temperatures than conventional ceramic-based TBCs and thus the heat loss reduction of SiRPA is greater comparatively. During post-combustion, it was observed that SiRPA coated surface followed the transient gas temperature path and reached a minimum temperature lower than ceramic TBCs, as shown in Figure 1. Therefore, SiRPA coating aids in preventing the preheating of incoming air during the intake stroke and reduces NOx emissions. It has been experimentally verified that SiRPA coatings have improved the fuel economy by 5.1% and reduced the NOx by 10% [8].

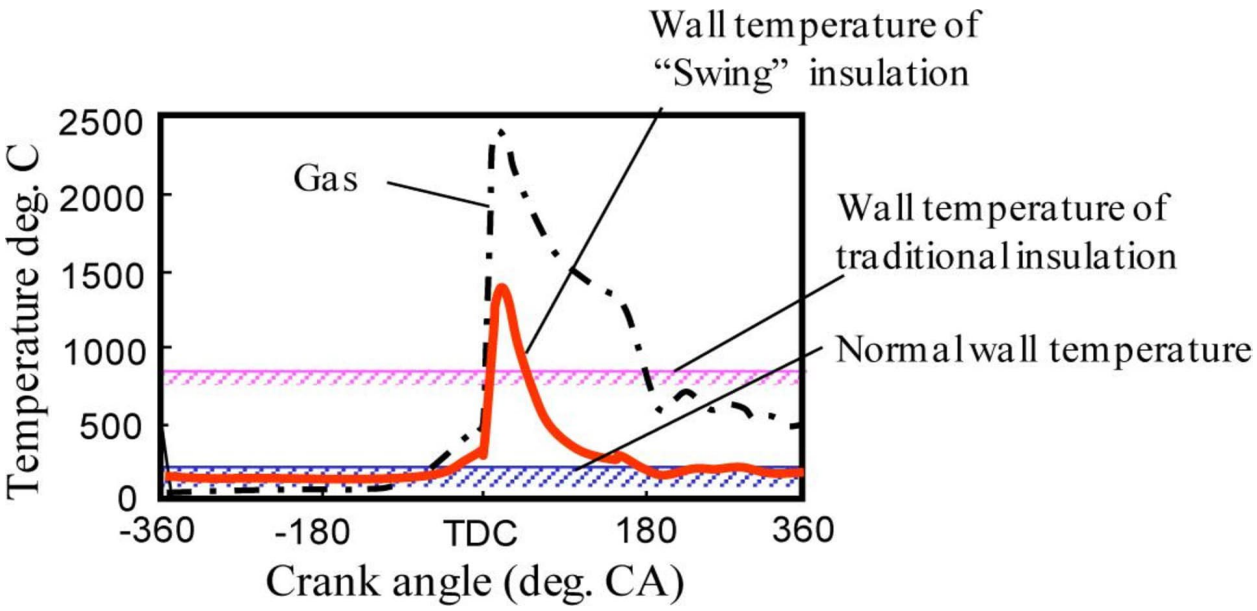

Figure 1: Engine wall temperature evolutions with different heat insulations. Reprinted with permission from [9]. Copyright 2013 SAE International.

SiRPA coating has the advantage of low volumetric heat capacity accompanied by low thermal conductivity, while YSZ based TBC has high volumetric heat capacity. This leads SiRPA to have higher temperature fluctuation compared to YSZ. In Ref.[9], two hypothetical cases were developed by scaling down thermophysical properties of YSZ (1/16 in case-1 and 1/32 in case-2) and compared with the baseline YSZ properties, to observe the effect of reduced thermophysical properties over temperature fluctuation. The temperature history clearly shows that as the volumetric heat capacity decreases, the temperature fluctuation increases. Since SiRPA has reduced thermophysical properties, therefore, a direct comparison of actual properties of YSZ and SiRPA is highlighted in current research to verify the effect of the low volumetric heat capacity of SIPRA on the difference in temperature fluctuation.

SiRPA coatings can be formed by the anodization process, and the temperature swing response or heat loss reduction largely depends upon the morphology and the porosity of the coating. Morphology is referred to the cell dimensions like pore diameter, inter pore distance, and barrier layer thickness. It is important to note that the coating morphology is highly dependent upon the anodization process parameters, like electric current density, anodization potential, anodization time, type of acid used, and concentration of the acid.

By controlling anodization process parameters, various configurations of SiRPA can be obtained by physical experimentation. Then using temperature measurement techniques, the thermophysical properties of these configurations can be obtained, along with the insulation performance of each coating configuration, to select the optimum morphology. The

thermophysical properties and overall morphology govern the insulation performance of the SiRPA coating.

Several studies are using the Conjugate Heat transfer (CHT) modeling technique which combines heat transfer in solids and fluids. It enables the user to predict the insulation performance like heat loss reduction, NOx formation, etc., for a given set of thermophysical properties of the coating [9]. However, these models rely on the thermophysical properties derived by physical testing, which involves intensive experimental efforts.

In this work, we will develop a computational model of the SiRPA coating using the FE based method to understand its temperature swing effect. Compared to previous work, this study will develop a full-scale 3D FE model that allows to accurately predict the thermophysical properties, and compare with the experimentally measured properties. Also, the specific set of geometric parameters in the FE model is derived from an experimentally developed coating. This makes a useful correlation between the coating fabrication parameters with the resultant SiRPA structures used in the model. In Section 2, the SiRPA coating growth mechanisms will be reviewed. In Section 3, the details of the FE model is presented. In Section 4, three different analyses using the FE model are discussed, including thermophysical properties, porosity-dependent thermal conductivities, and temperature swinging effect. In Section 5, the modeling results and discussion are presented, and a comparison with literature data is conducted when possible. Finally, the conductions are given in Chapter 6.

2. SiRPA coating growth mechanisms

SiRPA coating is grown as a result of the anodization process by immersing the aluminum into an acid electrolyte bath and passing an electric current through the medium. Typically, sulphuric acid, phosphoric acid, and oxalic acid are used. Sulphuric acid is widely used because it produces coatings at relatively low voltages [10]. During ionization, the ionic current results in the cooperative transport of (Al^{3+}) and (O^{2-}) ions with outward migrating (Al^{3+}) ions and inward migrating (O^{2-}) ions forming the film. The presence of an electric field produces a strong electrostriction pressure. As the thickness of the aluminum oxide layer increases, the compressive stress increases, and at a limiting oxide thickness when the stresses exceed the mechanical strength, the oxide undergoes mechanical breakdown and plastic flow leading to a pore. The development of the porous structure is therefore associated with continuous mechanical breakdown accompanied by continuous plastic flow. Figure 2 shows the schematic of the growth mechanism of pores[11].

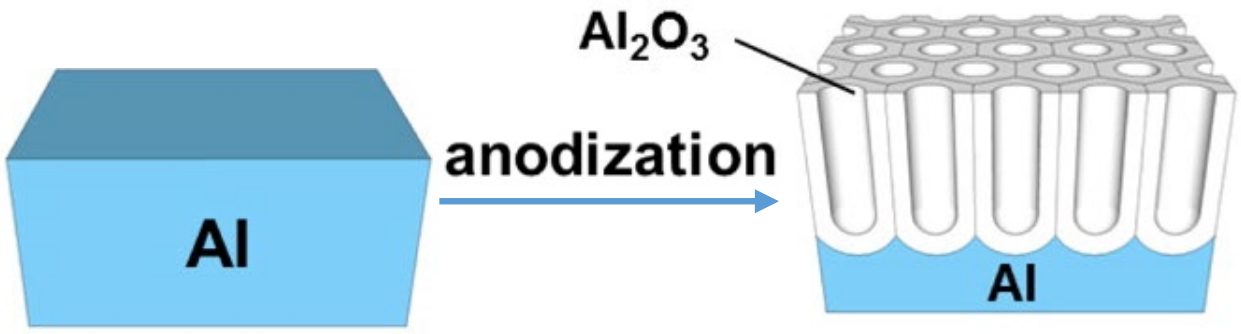

Figure 2: Growth mechanism of Porous Anodized Aluminum (PAA) coating [11]. Reprinted with permission from [11]. Copyright 2014 American Chemical Society.

As shown in Figure 2, the resultant Porous Anodized Aluminum (PAA) has a honeycomb-like structure containing many mutually parallel pores. Each cylindrical nanopore and its surrounding oxide constitute a hexagonal cell aligned normal to the metal surface[12]. The pores are aligned in a close-packed pattern in a process of relieving the film stress. The PAA microstructure is shown in Figure 3 [13].

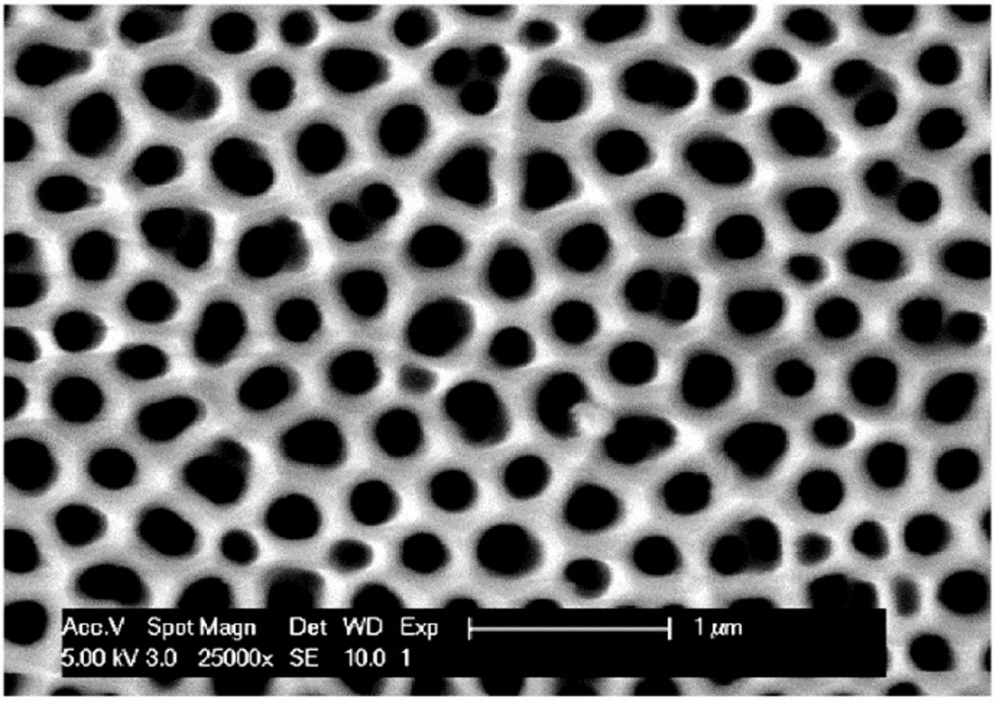

(a)

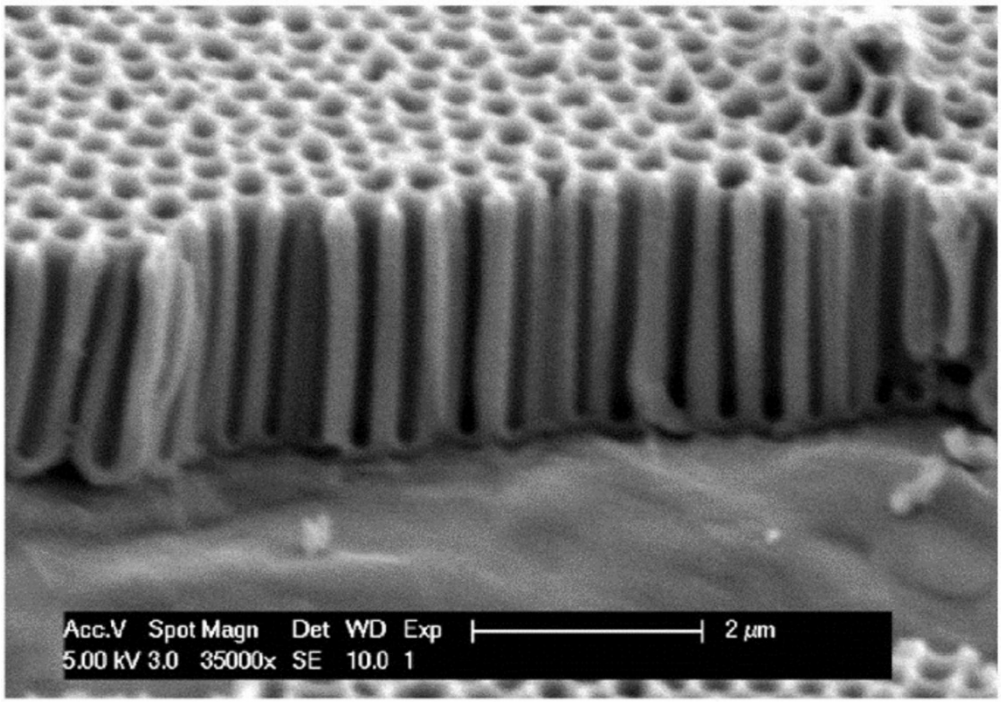

(b)

Figure 3: SEM images of PAA showing (a) top surface, (b) side view. Reprinted with permission from [13]. Copyright 2013 American Chemical Society.

IC engine pistons are Al-Si alloys, and in presence of silica, the porous structure grows in such a way that it avoids silica forming a micropore, as shown in Figure 4. These micropores can contribute 40% of the porosity. Together with cylindrical nanopores of oxide, PAA film can be 50% porous [14]. It is the amorphous nature of Al_2O_3 due to anodization and overall porous morphology of the structure that results in significantly low thermal conductivity, low heat capacity, and better heat loss insulation compared to traditional zirconia-based thermal barrier coating. Further to avoid the intrusion of the gas, a silica coat is also applied, sealing the topcoat and reinforcing the porous alumina as well [14].

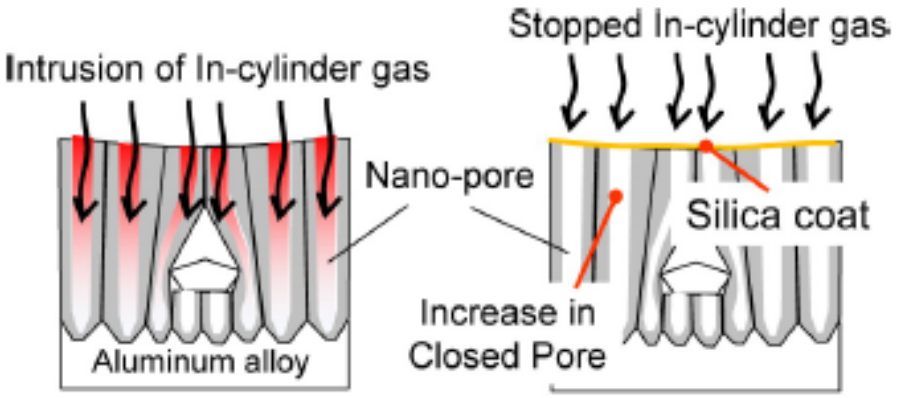

Figure 4: Schematic diagram of SiRPA on aluminum alloy substrate. Reprinted with permission from [14]. Copyright 2016 SAE International.

3. Finite element model details

3.1 Governing equations

According to the first law of thermodynamics, the amount of work W, wall heat loss Q_w, and exhaust loss H_{exh} equals the fuel heat input of engine Q [15]:

$$Q = W + Q_w + H_{exh} \quad (1)$$

During the combustion, the instantaneous heat flux through the wall is determined using the coupling Equations 2 and 3, which describe the unsteady thermal conductivity inside the wall and the heat transfer at the wall surface [6]. Now, if the heat flux through the wall is reduced, a reduction in the heat lost from the combustion chamber can be achieved, by varying either h, k, or ΔT [16]:

$$q_B = h\,(\Delta T) \quad (2)$$

$$\rho c\,(\partial T/\partial t) = k\,[\,\partial^2 T/\partial x^2 + \partial^2 T/\partial y^2 + \partial^2 T/\partial z^2\,] + s \quad (3)$$

where q_B = heat flux at the wall, h = heat transfer coefficient, k= thermal conductivity, ΔT = temperature difference between Tf (fluid) and Tb (combustion chamber wall surface), s = source of heat generation or loss.

The intake air temperature is raised which leads to shorter ignition delay, resulting in a larger rate of diffusion combustion and increased gas viscosity. This led to slower mixture formation and longer combustion period time. As a result, the fuel consumption has deteriorated, furthermore leading to increased NOx and smoke increased due to higher gas temperature and deteriorated mixture [17].

In an IC engine due to the periodic nature of the conduction heat transfer, thermal diffusivity (α) plays a significant role to capture the unsteady heat transfer and is given in Eq.4 below.

$$\alpha = k/ \rho c \quad (4)$$

It describes how quickly a material reacts to the change in external temperature and is equal to thermal conductivity divided by the volumetric heat capacity. Therefore, a material with the lowest volumetric heat capacity will reach a steady-state condition faster[18].

Another significant material property is effusivity (e) of a material, which determines a material's ability to exchange thermal energy with surrounding and is equal to the square root of the product of thermal conductivity (k) and the volumetric heat capacity (ρc) [5]:

$$e = \rho c*(\alpha)0.5 \quad (5)$$

Effusivity can thus be related to the heat flow (q) through a semi-infinite material initially at temperature To, placed in perfect thermal contact at time t = 0, with a thermal reservoir at temperature T1 > To, by Equation 2 [13]:

$$q = e\ (T1 - To) / t*(\pi)0.5 \quad (6)$$

Using a 1D simulation of heat transfer through the combustion chamber, the impact of thermo-physical properties over the temperature fluctuation was studied in Ref. [18]. The numerical model consisted of one-dimensional, axisymmetric, insulated piston substrate with the same thermal diffusivity that of YSZ, and geometry is assumed for piston surface temperature predictions. An engine cycle simulated was conducted, by varying the thermal effusivity for theoretical materials with fixed thermal diffusivity. It was thus observed that the theoretical material with the lowest effusivity resulted in maximum temperature during the power stroke with improved heat insulation. Therefore, a material with the lowest effusivity is desired which implies the requirement of an insulating technology with low volumetric heat capacity so that the combustion wall temperatures fluctuate rapidly with changing transient gas temperatures.

3.2 Determination of geometry parameters of SiRPA

In this research, a unit cell of the coating morphology is considered for computing the thermophysical properties. A CAD model is developed, and the geometry parameters are based on the morphology of a coating fabricated described in Refs.[7, 8]. The coating thickness was 0.1 μm with a pore diameter (Dp) 30 nm of the nanopore, which corresponds to the processing conditions of anodization conducted in 10% sulphuric acid with 30 mA/cm^2 current density. The porosity contributed by nanopore and micropore is 10% and 40% porosity respectively.

Now based on the given dimensions of pore diameters and interpore distance, anodization process parameters like the anodization potential and other coating geometric features like the barrier layer thickness can be determined. Generally, for porous anodized alumina, the dependency of pore diameter (D_p) and interpore distance (D_{int}) with anodization potential is linear. Equations 7 and 8 represent this relation where λ_p and λ_c are proportionality constants with 1.29 nmV^{-1} and 2.5 nmV^{-1} respectively [19]. In this work, the anodizing potential (U) is calculated to be 23 V and, from Equation 7 interpore distance (D_{int}) is 58 nm.

$$D_p = \lambda_p.U \quad (7)$$

$$D_{int} = \lambda_c.U \quad (8)$$

$$D_p = D_{int} - 1.42 \times T_b \quad (9)$$

$$\%P = 0.907 \times (D_p/D_{int})^2 \times 100 \quad (10)$$

The thermal barrier layer thickness T_b is calculated by using Equation 9 and it is 20 nm. The porosity (%P) of the cell is also evaluated to be 24% using Equation 10. Although in the literature referred, micropore contributes 10%, but it has been observed that the porosity measurement has great inconsistency, where the range varies from 8% to 30% [19], therefore it is reasonable to have a deviation of 14% from the literature values.

3.3 CAD model of SiRPA

The geometry of SiRPA consists of an aluminum substrate at the bottom, PAA in the middle, and silica coat over top. Based on the calculated D_{int}, a hexagonal cell of PAA with side = $D_{int}/\sin(60^o)$, with a pore in the center having diameter = $D_{p,}$ and barrier layer Tb is developed. Along with the nanopore at the center of each hex cell, a micropore is also included by modeling 30 cells hex cell, such that except peripheral cells, remaining cells are sliced and a micropore is created, as shown in Figure 5. It was required that the total porosity be around 50%, therefore an overall total porosity of 49.3% was achieved by varying the height of the unit cells which led to an increase in the void volume. Also, a silica topcoat that penetrates the nanopore was added, the depth of which was limited to achieve 49.3% porosity. The CAD model is designed in ANSYS Design Modeler software, and the FE model of the SiRPA model was built in ANSYS Workbench software.

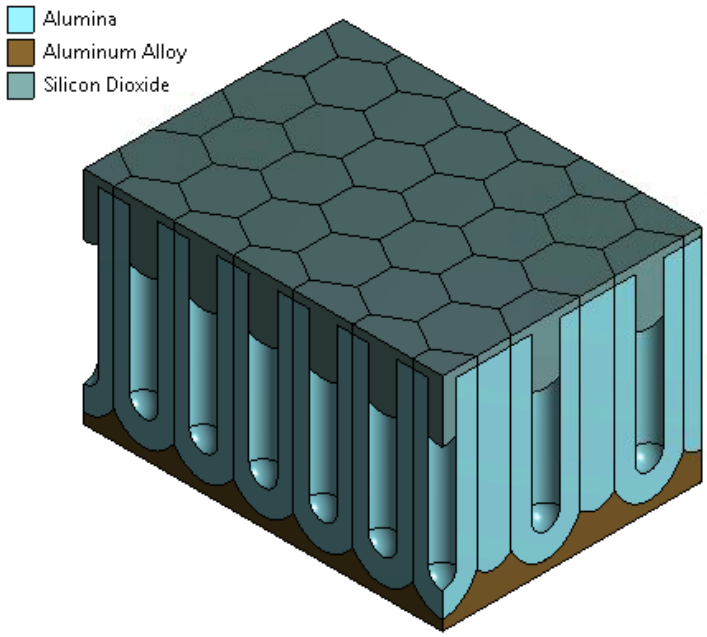

(a)

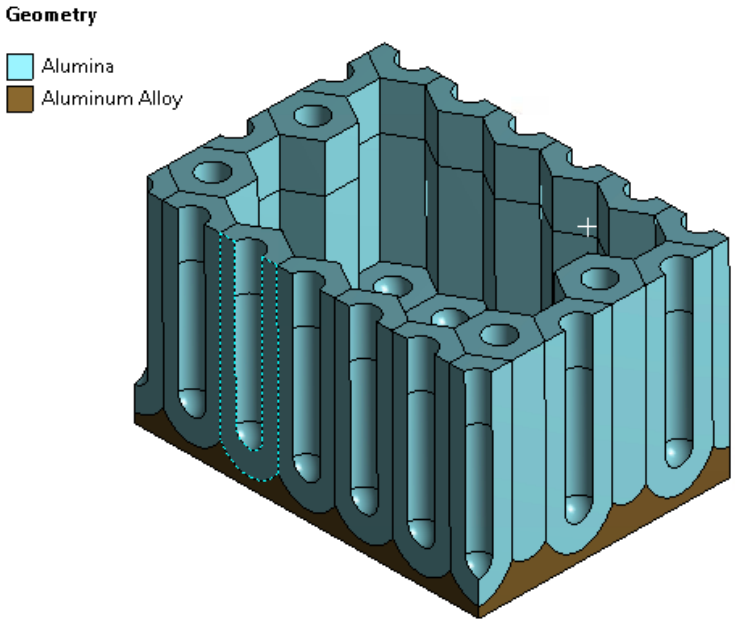

(b)

Figure 5: CAD model unit cells of SiRPA coating. (a) whole-cell model, (b) top silica layer removed to illustrate the internal structure.

3.4 Finite element mesh

The model was meshed using 3D quadratic tetrahedral elements, with total nodes 336,180. Figure 6 represents the FE model.

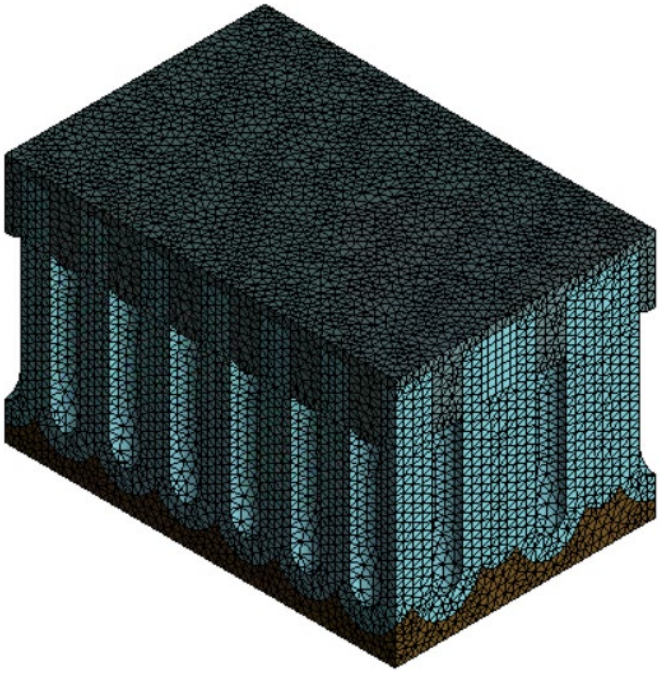

Figure 6: FE mesh of the unit cell of SiRPA coating

4. Finite element analysis

4.1 Prediction of thermophysical properties of SiRPA coatings

Based on the Refs. [7], [8], [14], the thermophysical properties of SIRPA material were determined by coating 100 μm thick SiRPA over an Al-Si alloy piston of a four-cylinder turbocharged diesel engine. The thermal conductivity λ and volumetric heat capacity Cv are estimated from bulk density ρ, specific heat capacity C, and thermal diffusivity D, as measured at 500 K, for which the temperature corresponds to the piston temperature after warming up. ($C_v = \rho \times C_p$, $\alpha = C_v \times D$). The specific heat capacity C is measured by differential scanning calorimetry (DSC). The thermal diffusivity of SiRPA is solved analytically from the measured thermal diffusivity of a double-layer test piece with a SiRPA and aluminum alloy substrate using a laser-flash methodology[14].

A steady-state thermal analysis using the FE model in Figure 6 is conducted to predict the thermophysical properties. The boundary conditions are such that the coating top face is at 227 ºC and the bottom is at room temperature 22 ºC. The boundaries are chosen according to physical testing conditions. The thermal conductivity K is calculated using Fourier's law of heat conduction. The heat flux is computed by considering the surface area of the topcoat, and the temperature

gradient is considered for the total thickness of the coating from the model. Material properties for each of aluminum, PAA, and silica are tabulated in Table 1 below.

Table 1: Thermophysical properties of Al, PAA, and SiO_2

Property	Al [20]	PAA [21]	SiO_2 [22, 23]
Specific heat Cp (J/kg-K)	875	755	1000
Density (kg/m^3)	2770	2950	2200
Thermal conductivity (W/m-K)	140	1.65	1.40

4.2 Parametric study of the effect of porosity on coating conductivity

As discussed in Section 2, the total porosity is contributed by nanopores and micropores. The micropore formed due to the presence of silica can vary in volume depending on the size of the Si-precipitate and affect the overall thermal conductivity of the SIRPA coating. Therefore, a parametric study is done in this section to quantify the variation in micropore porosity, and a mathematical expression is formed from the trend to predict the thermal conductivity of the coating.

In the FE model, the nanopore dimension is kept constant with porosity 24% [14] and the micropore volume is altered by varying the height in the empty region (micropore) of the cell, and different morphologies are designed similar to Figure 5.

4.3 Temperature swing effect simulation

A transient thermal analysis is conducted to simulate the temperature swing effect by comparing it with yttria-stabilized zirconia-based ceramic material [24]. The simulation is performed on a simplified geometry using a disk of 50 mm diameter and 300 μm thickness. The material properties of SiRPA are based on thermophysical properties predicted in this work. The thermal boundary condition is defined such that the top surface undergoes a cyclic thermal load. The temperature is raised from room temperature of 22 ^oC until 600 ^oC in 1 millisecond, then cooled in 1 millisecond at room temperature, followed by dwell of 1 millisecond at room temperature. 20 such cycles are simulated in both cases.

5. Results and discussion

5.1 Thermophysical properties

The predicted thermophysical properties are listed in Table 2, along with the experimental data. FEA closely predicts the thermal conductivity, bulk density, and diffusivity of SiRPA coating with experimentally obtained properties [8, 9, 14] at 500 K.

Table 2: Predicted thermophysical properties of SiRPA coating

Property	SiRPA: FEA (this study)	SiRPA: Experimental [8, 9, 14]
Specific heat Cp (J/kg-K)	922	929
Density (kg/m^3)	1504	1400
Volumetric Heat Capacity (KJ/m^3-K)	1589	1300
Thermal Conductivity (W/m-K)	0.67	0.67
Diffusivity (mm^2/s)	0.46	0.52
% Porosity	49	50

5.2 Porosity-dependent thermal conductivity

As discussed previously, the total porosity is contributed by nanopores and micropores. The micropore formed due to the presence of silica can vary in volume depending on the size of the Si-precipitate and affect the overall thermal conductivity of the SIRPA coating. Therefore, a parametric study is done in this section to quantify the variation in micropore porosity, and a mathematical expression is formed from the trend to predict the thermal conductivity of the coating.

In the FE model, the nanopore dimension is kept constant with porosity of 24% and the micropore volume is altered by varying the height in the empty region (micropore) of the cell. A variation in the thermal conductivities of each case of SiRPA morphology is plotted against variation in micropore porosity and an expression is obtained using the trendline. Equation (8) thus corresponds to the linear relation derived from the trend.

$$\%P_{total} = \%P_{micropore} + \%P_{nanopore} \quad (11)$$

$$K_{SIRPA} = - 0.012*(\%P_{total}) + 1.2597 \quad (12)$$

Thus, using Equations (4)-(7), nanopore porosity can be calculated based on anodization process parameters, and further extending to Equations 11 and 12, the thermal conductivity of SiRPA coating can be predicted. As shown in Figure 7 the thermal conductivity decreases linearly with increasing total porosity, following Equation 12.

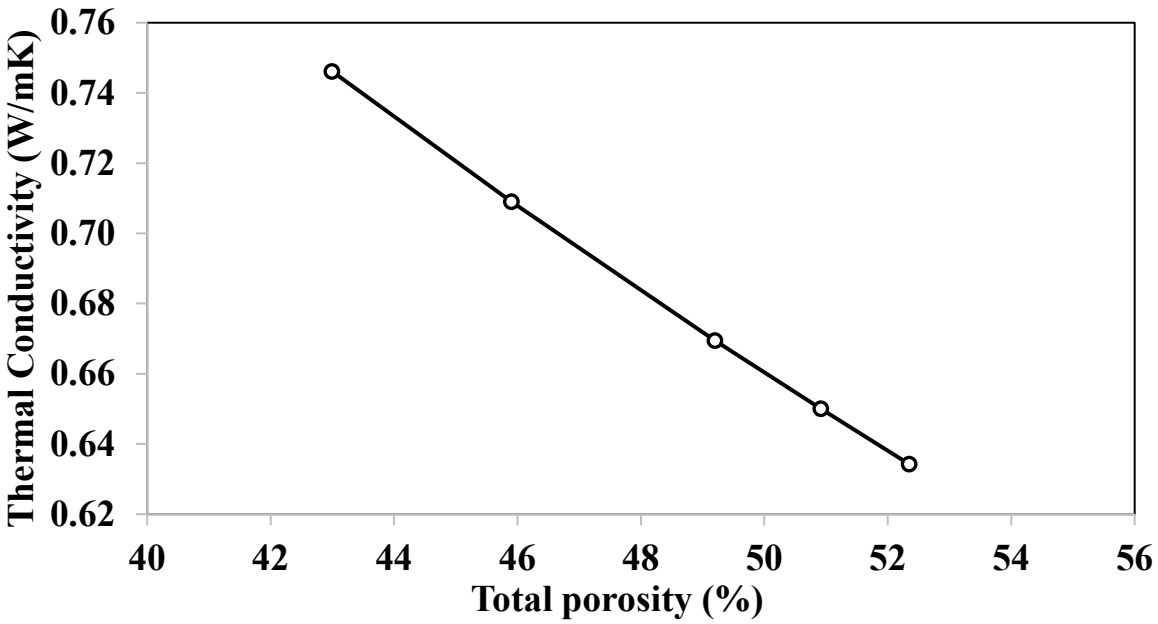

Figure 7: Predicted porosity-dependent thermal conductivity of SiRPA.

5.3 Temperature swing effect simulations

The temperature responses of the initial four cycles for the SiRPA, YSZ, and also input temperature are plotted in Figure 8. It can be seen from the response of transient thermal analysis that the maximum temperature attained by SiRPA during the heating phase is greater than YSZ, also during the cooling phase, the minimum temperature attained by SiRPA is lower than YSZ. Thus, temperature fluctuation is calculated by considering the difference in the maximum and minimum temperatures of both the coating material at the end of the heating and cooling phase in each cycle. An average temperature fluctuation of 20 cycles is then evaluated. The average temperature fluctuation of SiRPA coating is 226 ^{o}C and that of YSZ is 148 ^{o}C. SiRPA coating thus fluctuates 53% more than YSZ. Therefore, the predicted values can simulate the "temperature

swing" effect. More complex analysis can be performed in the case of coating applied over piston surfaces using a conjugate heat transfer model.

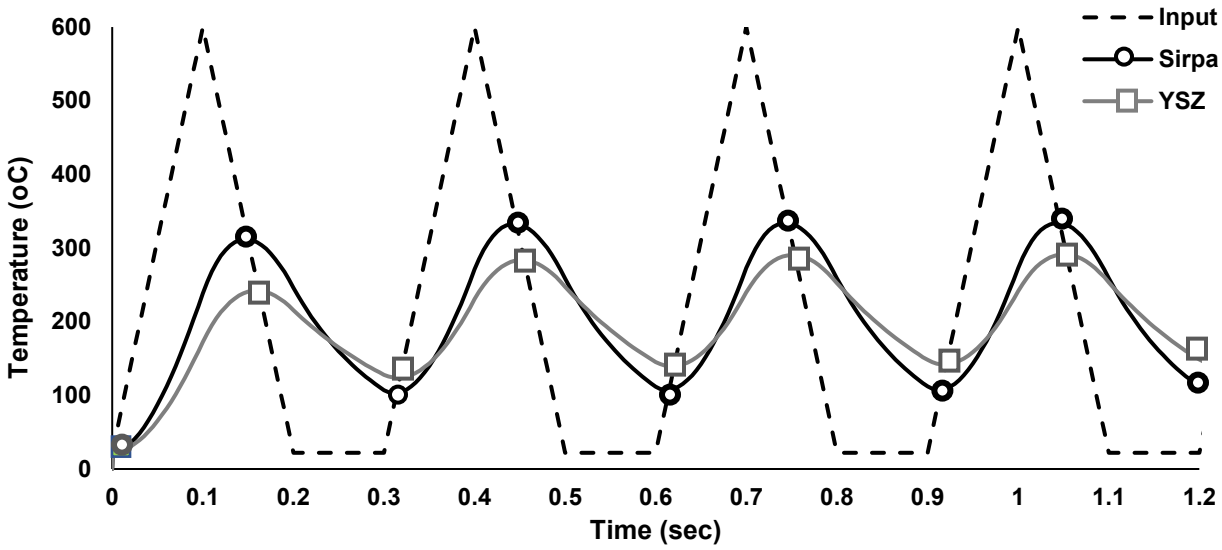

Figure 8: Comparison of temperature response fluctuation of SiRPA and YSZ coatings. The temperature input is also given.

In future work, this model can be extended to develop any morphology suitable for different combustion thermal conditions. An optimal thermal conductivity and heat capacity are required, which can be computed by conjugate heat transfer models [5] and 2D FE based transient heat conduction model [7]. Based on target thermal conductivity and volumetric heat capacity, a 3D morphology can be predicted by parametrizing the porosity. Thus from the predicted morphology the anodization process parameters can be set based on the empirical relations between the geometrical and process parameters[8]. Hence this technique can reduce experimental efforts of testing to find optimum coating morphology.

6. Conclusions

In this work, a FE model with a realistic microstructure of SiRPA is developed. The major conclusions are summarized as follows.

1. With the predicted thermophysical properties, the model is capable to predict the "temperature swing" effect of SiRPA by a transient thermal analysis. Temperature fluctuation of SiRPA is found greater compared to YSZ coating, suggesting its applicability in internal combustion engines.
2. The porosity-dependent thermal conductivity of SiRPA coating is numerically derived. The thermal conductivity decreases linearly with increasing total porosity.

3. The developed FE model can be used as a coating design tool. Specifically, the modeling approach can be adapted to determine the thermophysical properties of the SiRPA coating before its fabrication. Additionally, the FE model can be extended to develop any morphology suitable for different combustion thermal conditions. An optimal thermal conductivity and heat capacity are required, which can be computed by conjugate the heat transfer models, and the FE based transient heat conduction model. Hence this modeling technique can reduce experimental efforts of testing to find optimum coating morphology.
4. This model can be used for designing a realistic coating structure based on experimentally developed coating and anodization parameters. It can predict the thermophysical properties of SiRPA coating, and the predicted values are in good agreement with experimental measurements. However, the methodology has been tested only with one case of SiRPA morphology and needs further introspection with different morphologies.

Acknowledgments

This work is partially supported by the "Human Resources Program in Energy Technology (No. 20194030202450)", Power Generation & Electricity Delivery grant (No. 20181110100310)" of the Korea Institute of Energy Technology Evaluation and Planning (KETEP). Zhe Lu acknowledges the support provided by the National Natural Science Foundation of China (No. 51702145).

Conflict of interest statement

On behalf of all authors, the corresponding author states that there is no conflict of interest.

References

1. Kundu, P., et al., *Modeling Heat Loss through Pistons and Effect of Thermal Boundary Coatings in Diesel Engine Simulations using a Conjugate Heat Transfer Model*. 2016, SAE International.
2. Borman, G. and K. Nishiwaki, *Internal-combustion engine heat transfer.* Progress in Energy and Combustion Science, 1987. **13**(1): p. 1-46.
3. Inagaki, K., et al., *Low Emissions and High-efficiency Diesel Combustion using Highly Dispersed Sprays with Restricted In-cylinder Swirl and Squish Flows - Proposal of Combustion Concept and Validation of Fundamental Engine Performance using Single-cylinder Engine.* Transactions of Society of Automotive Engineers of Japan, 2011. **42**(1): p. 219-224.
4. Kikusato, A., K. Jin, and Y. Daisho, *A Numerical Simulation Study on Improving the Thermal Efficiency of a Spark Ignited Engine --- Part 1: Modeling of a Spark Ignited Engine Combustion to Predict Engine Performance Considering Flame Propagation, Knock, and Combustion Chamber Wall*. 2014, SAE International.
5. Matsuoka, H., et al., *Structure and performance of heat insulated natural gas engine.* JSAE Review, 1997. **18**(4): p. 377-384.
6. Kikusato, A., et al., *A Numerical Simulation Study on Improving the Thermal Efficiency of a Spark Ignited Engine --- Part 2: Predicting Instantaneous Combustion Chamber Wall Temperatures, Heat Losses and Knock*. 2014, SAE International.
7. Fukui, K., et al., *Development of Instantaneous Temperature Measurement Technique for Combustion Chamber Surface and Verification of Temperature Swing Concept*. 2016.
8. Kawaguchi, A., et al., *Thermo-Swing Wall Insulation Technology; - A Novel Heat Loss Reduction Approach on Engine Combustion Chamber*. 2016, SAE International.
9. Kosaka, H., et al., *Concept of "Temperature Swing Heat Insulation" in Combustion Chamber Walls, and Appropriate Thermo-Physical Properties for Heat Insulation Coat.* SAE Int. J. Engines, 2013. **6**(1): p. 142-149.
10. Ogden, T., *Thermal conductivity of hard anodized coatings on aluminum*, in *23rd Joint Propulsion Conference*.
11. Lee, W. and S.-J. Park, *Porous Anodic Aluminum Oxide: Anodization and Templated Synthesis of Functional Nanostructures.* Chemical Reviews, 2014. **114**(15): p. 7487-7556.
12. Lee, W., *Structural Engineering of Porous Anodic Aluminum Oxide (AAO) and Applications*, in *Nanoporous Alumina: Fabrication, Structure, Properties and Applications*, D. Losic and A. Santos, Editors. 2015, Springer International Publishing: Cham. p. 107-153.
13. Buijnsters, J.G., et al., *Surface Wettability of Macroporous Anodized Aluminum Oxide.* ACS Applied Materials & Interfaces, 2013. **5**(8): p. 3224-3233.
14. Wakisaka, Y., et al., *Reduction of Heat Loss and Improvement of Thermal Efficiency by Application of "Temperature Swing" Insulation to Direct-Injection Diesel Engines.* SAE Int. J. Engines, 2016. **9**(3): p. 1449-1459.
15. Somhorst, J., et al., *Experimental Evaluation of Novel Thermal Barrier Coatings in a Single Cylinder Light Duty Diesel Engine*. 2019, SAE International.
16. Kikusato, A., K. Jin, and Y. Daisho, *A Numerical Simulation Study on Improving the Thermal Efficiency of a Spark Ignited Engine --- Part 1: Modeling of a Spark Ignited Engine Combustion to Predict Engine Performance Considering Flame Propagation, Knock, and Combustion Chamber Wall.* SAE Int. J. Engines, 2014. **7**(1): p. 96-105.

17. Fukui, K., et al., *Development of Instantaneous Temperature Measurement Technique for Combustion Chamber Surface and Verification of Temperature Swing Concept*. 2016, SAE International.
18. Taibani, A., et al., *Analysis of Temperature Swing Thermal Insulation for Performance Improvement of Diesel Engines*. 2019, SAE International.
19. Abad, B., J. Maiz, and M. Martin-Gonzalez, *Rules to Determine Thermal Conductivity and Density of Anodic Aluminum Oxide (AAO) Membranes.* The Journal of Physical Chemistry C, 2016. **120**(10): p. 5361-5370.
20. Shah, R.K. and D.P. Sekulic, *Fundamentals of Heat Exchanger Design*. 2003: Wiley.
21. Al Mohtar, A., et al., *Thickness-dependent thermal properties of amorphous insulating thin films measured by photoreflectance microscopy.* Thin Solid Films, 2017. **642**: p. 157-162.
22. Grove, A.S., *Physics and technology of semiconductor devices*. 1967: Wiley.
23. *Material: Silicon Dioxide (SiO2), film (http://www.memsnet.org/material/silicondioxidesio2film/, accessed 3/8/2020)*.
24. Ekström, M., et al., *Evaluation of internal thermal barrier coatings for exhaust manifolds.* Surface and Coatings Technology, 2015. **272**: p. 198-212.